https://doi.org/10.5194/egusphere-2026-1910
Preprint. Discussion started: 4 May 2026

Barometric Pumping as a Driver of Subsurface CO_2 Emissions: A Comparative Study of Vadose Zone vs. Groundwater Wells

Ehud Lavner[1], Avner Gross[1], Uri Nachshon[2], Lior Netzer[3], Elad Levintal[4,*]

[1] The Department of Environment, Geoinformatics and Urban Planning Sciences, Ben-Gurion University of the Negev, Beer Sheva, 8410501, Israel
[2] Institute of Soil, Water and Environmental Sciences, Agricultural Research Organization, Rishon Lezion, 7505101, Israel
[3]The Hydrological Service, Israeli Water Authority, Jerusalem, 9195021, Israel
[4] Zuckerberg Institute for Water Research, the Jacob Blaustein Institutes for Desert Research, Ben-Gurion University of the Negev, Sde Boker campus, 8499000, Israel

Correspondence to: Elad Levintal (Levintal@bgu.ac.il)

https://doi.org/10.5194/egusphere-2026-1910
Preprint. Discussion started: 4 May 2026

Abstract. Wells can serve as conduits for gas exchange between the subsurface and the atmosphere. Yet, the controlling gas-transport mechanisms as a function of well type remain insufficiently understood. In this study, we identify and compare the controlling air transport mechanism between two infiltration well types located at the same site under similar soil and climatic conditions – a vadose zone well (i.e., dry well) and a groundwater well (i.e., wet well). During a 1-year experiment, high-resolution CO_2 and O_2 concentrations were measured at 1-minute intervals in each well, and atmospheric forcing was investigated using barometric pressure and temperature data. The dry well exhibited clear semi-diurnal cycles in CO_2 and O_2 concentrations that were coupled with fluctuations in atmospheric pressure, confirming barometric pumping (BP) as the dominant air transport mechanism. In contrast, the wet well showed no persistent diurnal oscillations. Instead, air transport was governed by seasonal processes: diffusion-driven stratification during summer and thermal-induced convection (TIC) combined with recharge-related dilution during winter. The groundwater table in the wet well acted as an impermeable boundary to BP, effectively suppressing advective gas exchange. From an environmental perspective, the dry well exhibits higher CO_2 emissions than the wet well, primarily due to the dominance of advective transport driven by BP, compared to the more diffusion-dominated transport (with a minor seasonal TIC addition) in the wet well. These results demonstrate that well type strongly controls air transport mechanisms and associated CO_2 emissions.

1. Introduction

The Earth's surface forms a dynamic boundary characterized by continuous gas exchanges between the critical zone and the overlying atmosphere. Numerous studies have investigated air transport between the subsurface and the atmosphere in a range of terrestrial environments, including porous soils (Du et al., 2023; Ganot et al., 2014; Smagin and Karelin, 2021; Smith et al., 2018) and subsurface cavities (Bourges et al., 2014; Dumitru et al., 2015; Liñán et al., 2025; Xiong et al., 2025). However, only a limited number of studies have examined the role of wells in facilitating or influencing subsurface–atmosphere gas exchange (Kang et al., 2014; Lebel et al., 2020; Levintal et al., 2018a; Levintal et al., 2020a; Levintal et al., 2020b; You et al., 2011). These studies have shown that such wells, dug for water or fossil fuel extraction, can be "hotspots" of greenhouse gas (GHG) emissions and serve as "conduits" that allow air transport between the subsurface and the atmosphere.

As global concern grows over climate change driven by increasing levels of GHG, such as carbon dioxide (CO_2) and methane (CH_4), it has become clear that abandoned oil and gas wells can be significant sources of these emissions. In California, Lebel et al. (2020) reported significant CH_4 emissions (35.4 g/hr) from approximately 124,000 abandoned oil and gas wells. Similarly, Kang et al. (2016) estimated that there are 470,000-750,000 abandoned wells in Pennsylvania, which contribute 5-8 % of the state's annual anthropogenic CH_4 emissions. Although there are many oil and gas production wells in the United States and around the world, there are even more wells of other types, for example, for pumping drinking water from shallow aquifers (tens of meters). Only a few studies have investigated emissions from these types of wells, with one showing significant CO_2 emissions from a single groundwater well at a magnitude similar to that of an average wheat field, approximately 1000 to 6000 m^2 in size (Levintal et al., 2020b).

https://doi.org/10.5194/egusphere-2026-1910
Preprint. Discussion started: 4 May 2026

Humans have been using wells for water since the beginning of their existence. Even today, a significant portion of the world's population still relies on water from shallow wells for drinking, irrigation, and other purposes (Misstear et al., 2017). Only in the United States there are more than 15.9 million wells, with about 500,000 new wells being constructed every year (National Ground Water Association [NGWA]). There are many types of wells, each having a slightly different purpose. One such type is the infiltration well, which is used for managed aquifer recharge (MAR), a method of introducing surface water into the subsurface for groundwater recharge.

There are wells that go down to the unsaturated zone (dry wells), and there are wells that reach directly into the aquifer (wet wells) (Netzer et al., 2024). Infiltration wells are important, especially in urban areas, where a significant portion of the surface is impermeable to infiltration. In urban environments, infiltration wells divert surface water during rain events into the subsurface, mitigating urban flooding, replenishing groundwater with high-quality water, and alleviating the burden on municipal drainage systems (Liang et al., 2018; Netzer et al., 2024). Because these wells are directly open to the atmosphere, they may act as efficient conduits for the exchange of gases, enabling GHGs to migrate from the subsurface to the atmosphere with minimal resistance. This structural openness facilitates rapid air transport, especially under dynamic atmospheric conditions, such as fluctuations in barometric pressure.

Infiltration wells, as well as other types of wells, allow the transport of air between the subsurface and the atmosphere. This open path may result in the release of CO_2 (Levintal et al., 2020b), CH_4 (Gora et al., 2018), and other GHGs into the atmosphere. There are two potential sources of these gases in wells: groundwater at the well bottom (Minamikawa et al., 2010; Morais & Ryan, 2023) and the unsaturated zone above the groundwater table surrounding the perforated section of the well (Levintal et al., 2018b). The dissolved CO_2 ($CO_{2(aq)}$) in groundwater has a partial pressure one to two orders of magnitude higher than that in the atmosphere (Macpherson, 2009), driving CO_2 degassing. There are several sources of CO_2 in groundwater and the unsaturated zone, including the respiration of plant roots or microbes, oxidation of recent organic carbon in the unsaturated zone, oxidation of old organic carbon in the aquifer matrix, and upward leakage of mantle or petroleum reservoir CO_2 (Macpherson, 2009).

The air within wells can freely exchange with the atmosphere. The dynamics of the atmosphere, through meteorological phenomena and climatic cycles, are one of the driving forces for air transport, controlling the magnitude and dominance of the various transport mechanisms (Levintal et al., 2020b; Perrier & Le Mouël, 2016). Two advective processes primarily govern air transport within wells. The first, barometric pumping (BP), involves the movement of air driven by fluctuations in barometric pressure (P_{atm}) (Jiang et al., 2023; Li et al., 2022; Mourzenko et al., 2014). The second mechanism, known as thermal-induced convection (TIC), results from density instabilities that arise due to temperature differences between the well environment (or other subsurface cavities) and the surrounding atmospheric air (Ganot et al., 2012; Nachshon et al., 2008; Weisbrod et al., 2009).

BP is a process in which P_{atm} fluctuations drive air transport between adjacent areas (Levintal et al., 2020b; Mourzenko et al., 2014; Rossabi & Falta, 2002). Air will flow to/from the well depending on the differential pressure between the gas pressure in the unsaturated zone surrounding the well and the

https://doi.org/10.5194/egusphere-2026-1910
Preprint. Discussion started: 4 May 2026

ambient atmosphere (You et al., 2010). As P_{atm} decreases (i.e., $dP_{atm}/dt < 0$), the air is drawn from the pore space at the unsaturated zone into the open well section, while P_{atm} increases (i.e., $dP_{atm}/dt > 0$), causing air to flow in the opposite direction, from the atmosphere into the well (Neeper, 2003). This cyclic exchange of gases depends on factors like the intensity and frequency of P_{atm} variability, the permeability and depth of the unsaturated zone surrounding the well, and the dimensions of the well and perforated section within (Levintal et al., 2018b; Massmann et al., 2000). BP can efficiently transport gases, such as CO_2, between the subsurface and the atmosphere, making it a key transport mechanism in wells (Perriaer & Le Mouël, 2016).

TIC is a process mainly determined by air density differences between the well's headspace above the groundwater table and the atmosphere above, and by vertical air density differences within the well (Levintal et al., 2018a; Ganot et al., 2012). To better explain the air's density differences, a parameter named virtual temperature (T_V) is used, accounting for the combined effect of temperature (T), relative humidity (RH), and the air's gas composition on the air density (Sánchez-Cañete et al., 2013). T_V represents the temperature of dry air that has the same density as a parcel of moist air at the same pressure and gas composition (Monteiro & Torlaschi, 2007). TIC may initiate when the virtual air temperature within the well is higher than that of the atmosphere above (i.e., $T_{Vwell} > T_{Vatm}$).

However, although air transport mechanisms in wells have been studied, the effect of the well's type (dry or wet) on the mechanisms and CO_2 emissions has not yet been examined. To address the limited understanding of gas exchange in infiltration wells, this study presents high-resolution, multi-depth, year-long monitoring of CO_2 and O_2 dynamics in two infiltration wells – a dry well and a wet well – located at the same site under identical soil and climate conditions. This unique comparative approach allows direct in-situ evaluation of the controlling air transport mechanisms, such as BP and TIC, as a function of well type. By quantifying CO_2 gas fluxes and identifying the dominant transport drivers, this study provides new insights into the role of infiltration wells in subsurface-atmosphere gas exchange and their potential contribution to GHG emissions.

2. Materials and Methods

2.1. site description

The research was conducted at the Volcani Research Center, located in central Israel, approximately 8 km east of the Mediterranean Sea (31.991245/34.820653) (**Fig. 1a**). The site overlies the coastal plain aquifer, which is an unconfined aquifer, composed mostly of sand and calcareous sandstone, with a thickness ranging from a few meters in the east to about 200 m at the coastline (Netzer et al., 2024). The average groundwater table at the site was -37.82 m below the ground surface. The climate is Mediterranean, characterized by wet winters and hot, dry summers (Lionello et al., 2006). The average precipitation in the area is 540 mm/year, with 56 rainy days on average per year (Israel Meteorological Service (IMS)).

In July-August 2020, two infiltration wells were drilled: a dry well and a wet, approximately five meters apart (**Fig. 1a**). The wet well is 47 m deep and perforated at the interval of 42–47 m below the ground

https://doi.org/10.5194/egusphere-2026-1910
Preprint. Discussion started: 4 May 2026

surface, whereas the dry well is 27 m deep and perforated at 22–27 m below the ground surface (**Fig. 1b**). In both wells, perforation is 11 %, with a 1 mm opening. Both wells consist of 0.203 m diameter PVC pipes. The annuluses around the tubes (diameter of 0.353 m) were filled with cement, excluding the levels of perforation that were filled with coarse sand-fine gravel at a diameter of 1.5–2.5 mm (Netzer et al., 2024). Since 2020, several controlled infiltration experiments have been conducted during the summer months, while the operational infiltration of harvested rainwater from an adjacent roof has been performed during the winter seasons, as detailed by Netzer et al. (2024, 2025). With respect to the period of the current study, on 07/11/2024, a controlled infiltration experiment was carried out on site, during which water was injected into the wet well for an hour at an average flow rate of 14.45 m^3/h. In addition, an operational infiltration through the wet well took place between 20/12/2024 and 29/05/2025. During this period, a 0.13-m-diameter pipe was installed in the upper section of the wet well to deliver harvested rainwater from the adjacent roof; the water was released into the well solely by gravity for MAR purposes. It is important to emphasize that the upper boundary of the well remained unsealed; even with the installation of the water inlet pipe, gas could exchange freely between the well and the atmosphere.

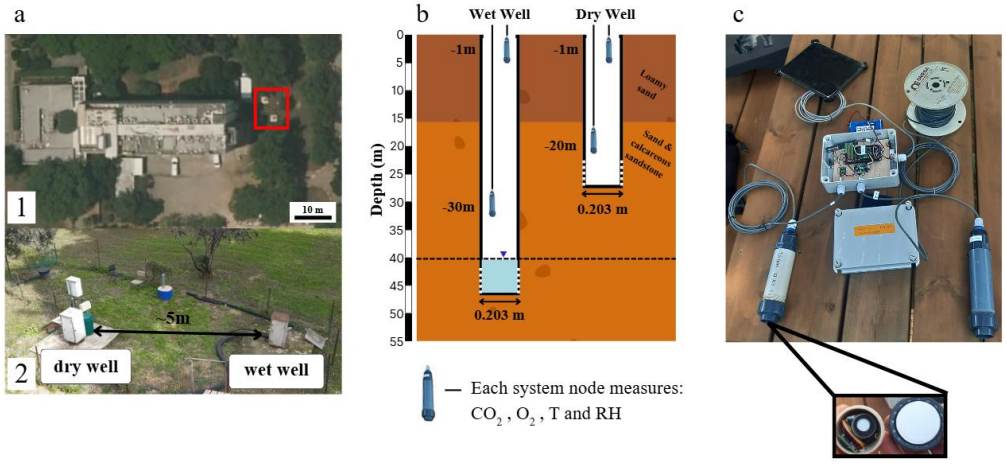

Figure 1: Experimental design. (a-1) The location of the infiltration wells in the red rectangle (taken from Google Earth, ©2026 Airbus, CNES), and (a-2) a picture of the infiltration wells. (b) Schematic sketch of the infiltration wells with sensors. The dashed horizontal line and blue triangle indicate the groundwater table. The dashed vertical lines at the bottom of both wells represent the perforated section. (c) Photos of the monitoring system before installation in the dry well. The system of the wet well is constructed similarly.

2.2. Sensor setup and data collection

On 27/08/2024, a novel high-resolution, real-time monitoring system was installed in both wells (**Fig. 1c**). Each system consists of two sensor nodes. Each sensor node was housed in a waterproof box that allowed gas exchange between the sensors and the surrounding air. Each sensor node transmitted the data to a data logger (Adalogger, Adafruit, USA) and to an online server (Notecard modem, blues.io, USA). Data was logged at 1-minute intervals. All system components were operated using a 3.7 V rechargeable

https://doi.org/10.5194/egusphere-2026-1910
Preprint. Discussion started: 4 May 2026

battery connected to a solar panel. Each node consisted of one sensor to measure CO_2, T, and RH (SCD30, Sensirion, Switzerland) and a second sensor to measure O_2 (Gravity, DFROBOT, China). In both wells, we placed one node at the top of the well, at -1 m (top node) and a second node at the bottom of the well, at -20 m in the dry well and at -30 m in the wet well (bottom node) (**Fig. 1b**).

To understand the mechanisms controlling air transport within the wells, we used data from a nearby meteorological station, Beit Dagan (IMS), located 1.9 km from the wells at a similar elevation (14 m elevation difference). The station recorded T, RH, precipitation, P_{atm}, and wind speed at 10-minute intervals.

The measurements lasted continuously for one year, from 02/09/2024 to 01/09/2025, with several periods without data due to technical malfunctions. The periods with missing data from the dry well are 15/12/2024-28/01/2025 and 03/07/2025-11/08/2025. The periods with missing data from the wet well are 10/09/2024-24/09/2024, 1-17/11/2024, and 13-23/02/2025.

2.3. Well survey measurements

Additional on-site measurements were conducted monthly to obtain vertical CO_2 profiles within the wells. For this purpose, a trace gas analyzer (LI-7810, LI-COR, USA) was used. The inlet tube connected to the gas analyzer was positioned for five minutes at each of the following depths, and the measured concentrations were recorded: surface air, -1, -5, -10, -15, and -20 m (and -25 m and -30 m in the wet well). In addition, we used a $CO_{2(aq)}$ probe (Solu-Blu™, Pro-Oceanus, Canada) to measure groundwater concentrations.

2.4. Quantifying CO_2 fluxes

2.4.1. Calculating air velocity using CO_2 data

High-resolution CO_2 measurements from the two sensor nodes installed in each well enabled the calculation of vertical air velocity within the well (V_{air}). Assuming advective transport, where CO_2 moves as part of a bulk air mass, V_{air} within the well can be calculated as follows (Levintal et al., 2020b): during upward air flow with high CO_2 concentrations from the groundwater or unsaturated zone (*outflow*), an increase in CO_2 concentration is expected to occur first at the bottom node, followed by the top node. The time lag between these responses represents the travel time of the air mass between the two points. Dividing the vertical distance between the nodes (19 m in the dry well; 29 m in the wet well) by this time lag yields the upward V_{air}. This method can also be applied to downward flow events to estimate the velocity of air with low atmospheric concentrations (~420 ppm) entering the well from the atmosphere (*inflow*). In this case, a decrease in CO_2 concentration is expected to occur first at the top node, followed by the bottom node.

2.4.2. Transforming CO_2 units from ppm to mass

To calculate the CO_2 fluxes, concentrations converted from units of ppm to units of mass (g/m^3) using the following equation:

https://doi.org/10.5194/egusphere-2026-1910
Preprint. Discussion started: 4 May 2026

$$[CO_2]_m = \left(\frac{[CO_2]_{ppm} \times M_{CO2} \times P}{R \times T}\right)\left(\frac{10^{-3}kg}{g}\right) \quad (1)$$

where $[CO_2]_m$ [g-CO_2/m^3] is the CO_2 concentration in mass, $[CO_2]_{ppm}$ [ppm] is the CO_2 concentration in ppm, M_{CO2} [g/mol] is the molar mass of CO_2 (44.01), P [Pa] is the pressure, R [m^3 Pa/(K*mol)] is the universal gas law constant (8.31451), and T [K] is the temperature.

2.4.3. CO_2 flux calculation

The flux was calculated as the V_{air} component multiplied by the cross-sectional area of the pipe (CO_2 flux across a plane, such as the well-atmosphere interface):

$$Q_{CO_2} = [CO_2]_m \times V_{air} \times A_{well} \quad (2)$$

where Q_{CO2} [g-CO_2/min] is the mass flux of CO_2, $[CO_2]_m$ [g-CO_2/m^3] is the CO_2 concentration measured at the top node in each well using **Eq. 1**, V_{air} [m/min] is the velocity of the air, (plus and minus signs represent *outflow and inflow* directions, respectively), and A_{well} [m^2] is the cross-section of the well at the well-atmosphere interface (0.03265 m^2).

2.5. Time-series analysis

All analyses and calculations were performed in Python, with key operations implemented using the scientific libraries NumPy, pandas, and SciPy (see **Fig. S1** in the supplementary information for the algorithm flowchart). The time-series data were first preprocessed to ensure analytical consistency. This included chronological sorting and smoothing of key variables (CO_2 and O_2 concentrations at both top and bottom nodes) using a 30-point rolling mean.

First-order numerical derivatives were computed for each smoothed signal to assess rates of change and identify local inflection points. For the dry well, the onset of increasing CO_2 concentrations (termed as valley points) was detected by locating zero-crossings in the derivative that marked transitions from decreasing to increasing CO_2, followed by a verification that the subsequent slope remained positive for at least 80 minutes. Similar logic was applied to identify peak points in the top node's CO_2, defined as the last data point before a sustained negative derivative (see **Fig. S2** in the supplementary information for an example). In contrast, such peaks and valleys analyses were not performed for the wet well's time-series, as its gas concentration profiles exhibited minimal short-term variation, suggesting an absence of consistent diurnal air transport (see the discussion in section 3 for more information).

Following the identification of valley and peak events in the dry well, valley points in the bottom node were temporally matched to subsequent valleys in the top node, constrained by a minimum separation of 40 minutes. These matched intervals were used to calculate V_{air} over the known vertical distance between sensors. *Outflow* events were defined as the intervals between a valley and its succeeding peak in the top node and were used to segment the data for further analysis (**Fig. S2**). In parallel, P_{atm} peaks were identified in meteorological data using peak prominence thresholds. Then, the temporal offset between pressure peaks and *outflow* initiation was quantified to investigate barometric forcing.

https://doi.org/10.5194/egusphere-2026-1910
Preprint. Discussion started: 4 May 2026

Frequency-domain characteristics of CO_2, O_2, temperature, and P_{atm} were analyzed using fast Fourier transform (FFT) (Perrier and Richon, 2010), with power spectra computed over positive frequencies and examined up to 10 cycles per day. The FFT is an extremely efficient algorithm used to compute the Discrete Fourier Transform (DFT) and its inverse. The primary purpose of the Fourier Transform is to decompose a signal (a function of time or space) into its constituent frequencies. In essence, it converts a signal from its original time-domain representation to a frequency-domain representation (Slade, 2013).

3. Results and Discussion

3.1. Time series data

Time series data at 1-minute intervals of O_2, CO_2, and ΔT_V within the wells, and the P_{atm} are presented in **Fig. 2** (dry well) and **Fig. 3** (wet well). In order to better discern trends, five representative consecutive days during June 2025 were selected. In the dry well, both CO_2 and O_2 concentrations exhibited clear semi-diurnal oscillations, but in opposite directions (**Fig. 2b** and **2c**). CO_2 concentrations at both the top (-1 m) and bottom (-20 m) nodes ranged from atmospheric background levels (~420 ppm) up to 40000 ppm, the saturation limit of the sensor. O_2 concentrations fluctuated between 16.3 % and the atmospheric baseline of 20.9 %. P_{atm} also exhibited semi-diurnal cycles, with an average value of 1005.8±0.99 hPa (**Fig. 2a**). The virtual temperature of the atmosphere (T_{Vatm}) was higher than that within the well at the bottom node ($T_{Vbottom}$) with an average difference ($\Delta T_V = T_{Vbottom} - T_{Vatm}$) of -5.62±4.18 °C (**Fig. 2d**).

In contrast to the dry well, gas behavior within the wet well showed markedly different trends (**Fig. 3b** and **3c**). At the bottom node (-30 m), CO_2 levels remained above the sensor saturation threshold (40000 ppm) throughout the observed period, indicating poor ventilation and persistent gas accumulation. Correspondingly, O_2 concentrations at the bottom remained low and stable, averaging 16.2±0.06 %. At the top wet well node (-1 m), CO_2 concentrations were low compared to the bottom wet well node with an average of 852±418 ppm, and O_2 concentrations with an average of 20.8±0.1 %. ΔT_V was lower than in the dry well, with an average of -7.87±3.25 °C (**Fig. 3d**).

https://doi.org/10.5194/egusphere-2026-1910
Preprint. Discussion started: 4 May 2026

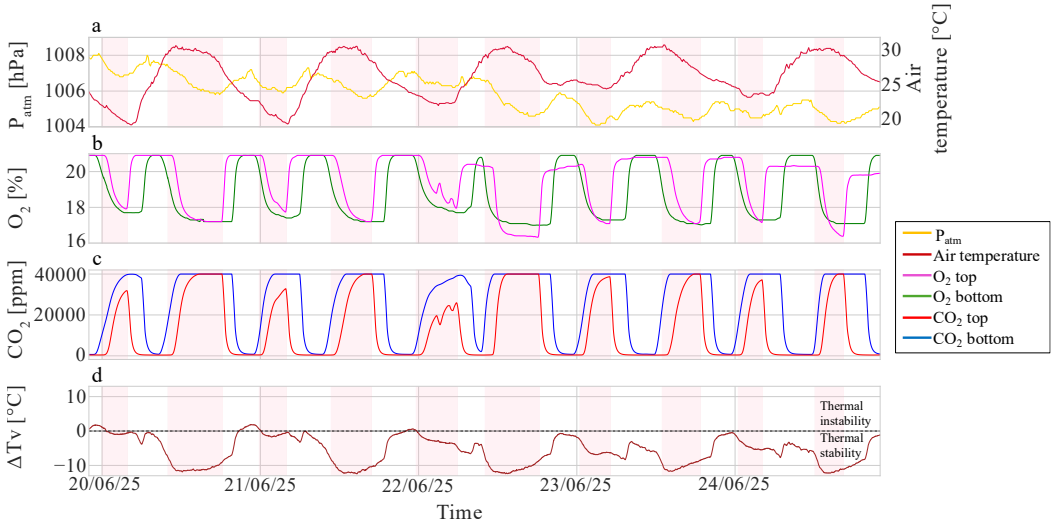

Figure 2: Time series data from five representative days for the dry well. ΔT_V represents the virtual temperature (T_V) differences between the bottom node of each well and the atmosphere ($T_{V(bottom)} - T_{V(atm)}$); positive ΔT_V means thermal instability. Top and bottom nodes correspond to -1 and -20 m, respectively. The pink-shaded areas represent *outflow* events.

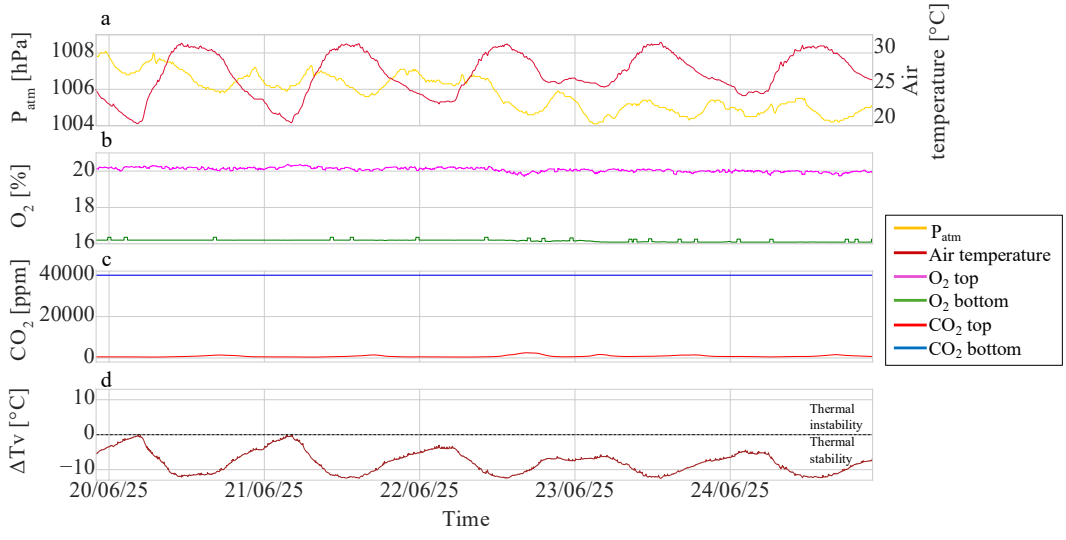

Figure 3: Time series data from five representative days for the wet well. ΔT_V represents the virtual temperature (T_V) differences between the bottom node of each well and the atmosphere ($T_{V(bottom)} - T_{V(atm)}$); positive ΔT_V means thermal instability. Top and bottom nodes correspond to -1 and -30 m, respectively.

The trend observed in the dry well over the five days shown in **Fig. 2** was also observed throughout the monitoring period (see **Fig. S3** in the supplementary information). The trend observed in the wet well

https://doi.org/10.5194/egusphere-2026-1910
Preprint. Discussion started: 4 May 2026

over the five days shown in **Fig. 3** was also observed during the warm months (April-October), whereas in the cold months (November-February), a different trend was observed, as discussed in Section 3.4.2.

3.2. Concentration vs depth

Vertical concentration profiles of CO_2 within the dry and the wet well, which were measured on specific sampling days (~1-month intervals), are presented in **Fig. 4**. In the dry well, the observed depth profile depended on the time of measurement. On days when the measurement was made in the early morning hours (7:00-10:30), during an *inflow* event, atmospheric values were observed at all sampling depths of the well (e.g., **Fig. 4a**, brown line). However, on days when measurements were taken in the late morning or afternoon (10:30-14:00), at the beginning or during an *outflow* event, CO_2 values increased with depth (e.g., **Fig. 4a**, blue lines).

The depth profiles of CO_2 in the wet well showed a different pattern (**Fig. 4b**). On all sampling days, CO_2 concentrations increased with depth, but the maximum values measured at the bottom of the well were seasonally dependent. On winter sampling days (November–February), CO_2 concentrations at a depth of -30 m were lower than on spring sampling days (March–May), which in turn were lower than on summer sampling days (June–August). A seasonal shift was also evident in the CO_2 transition layer depth, where concentration increases became most pronounced. In summer, this transition layer depth occurred closer to the surface (−5 to −10 m), while in spring and winter, it shifted deeper (around −20 m) or was absent altogether. In the latter cases, CO_2 concentrations increased more gradually with depth. These patterns suggest that in the wet well, warm atmospheric conditions strengthen stratification, limiting vertical mixing and allowing CO_2 to accumulate in the deeper layers, forming a linear concentration gradient.

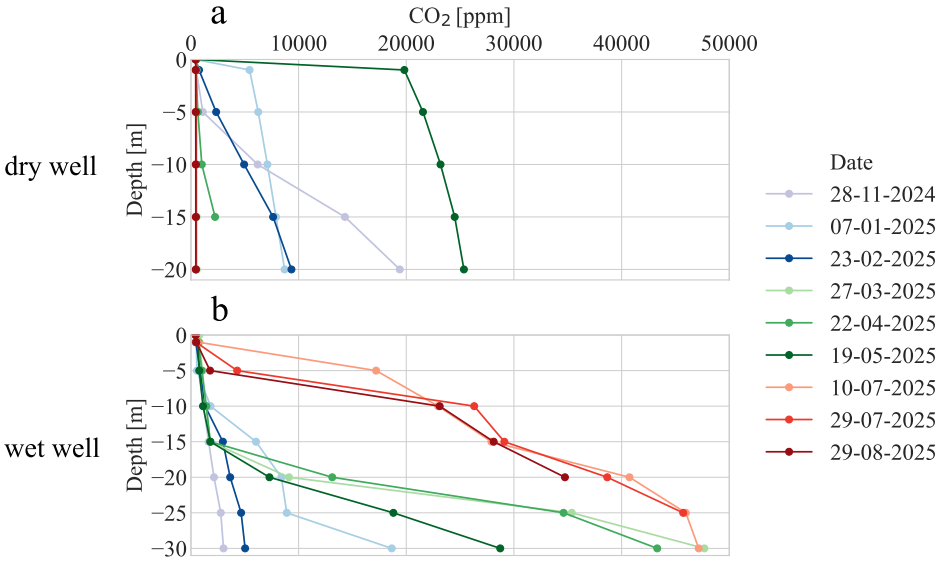

https://doi.org/10.5194/egusphere-2026-1910
Preprint. Discussion started: 4 May 2026

Figure 4: Depth profiles of the CO_2 concentration in (a) the dry well and in (b) the wet well. Each line represents a different sampling day. Blue lines represent winter months, green lines represent spring months, and red lines represent summer months. CO_2 concentrations were measured with the Trace Gas Analyzer (LI-7810, LI-COR, USA) (section 2.3).

3.3. Air velocities and CO_2 fluxes

Air velocities and CO_2 fluxes were calculated only for the dry well, as in the wet well, low CO_2 concentrations were measured at the top of the well, suggesting air stratification with negligible advective air velocities. Most *outflow* events in the dry well were characterized by air velocities ranging from 0.1 to 0.3 m/min, with the average air velocity calculated during the *outflow* events being 0.246 m/min (**Fig. 5a**). The flux per minute (using **Eq. 2**) and the cumulative flux over the entire measurement period are shown in **Fig. 5b**.

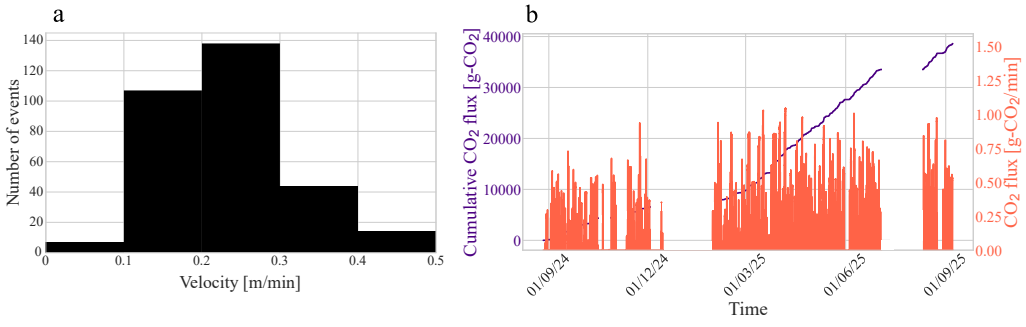

Figure 5: (a) Histogram of air velocities during *outflow* events in the dry well; (b) Continuous and cumulative CO_2 fluxes from the dry well during the experimental period. Blank areas indicate missing data due to system malfunctions (see section 2.2 for additional details).

The measured flux values are relatively lower than those of other wells. Levintal et al. (2020b) found that the CO_2 flux from an abandoned water well (110 m in depth and 1 m in diameter) reached up to 5 g-CO_2/min in the summer months, while the flux measured in the dry well usually did not exceed 1 g-CO_2/min. The lower CO_2 fluxes in the dry well are most likely due to relatively low air velocities (V_{air} parameter in **Eq. 2**) during the *outflow* events within the well (~0.2 m/s compared to >1 m/s in Levintal et al., 2020b).

3.4. Air transport mechanisms

3.4.1. Barometric pumping in the dry well

Fig. 6a shows CO_2 concentrations at the bottom and top nodes of the dry well, along with P_{atm}, over three representative days in June. Both CO_2 concentrations and P_{atm} exhibit clear semi-diurnal cycles, with two peaks per day. Notably, the onset of increasing CO_2 concentrations at the bottom node (valley points in **Fig. 6a**) consistently precedes the rise in CO_2 at the top node. This pattern indicates an *outflow* event, in which CO_2-rich air is first transported from the surrounding unsaturated zone into the bottom of the well through the perforated section and then up the well shaft to the atmosphere. Conversely, during *inflow*

https://doi.org/10.5194/egusphere-2026-1910
Preprint. Discussion started: 4 May 2026

events, the CO_2 concentration at the top node begins to decrease before changes are observed at the bottom node. This timing indicates the entry of atmospheric air into the well, displacing the internal gas downward into the surrounding unsaturated zone. Importantly, these air transport cycles are tightly coupled with P_{atm} fluctuations. The beginning of a P_{atm} decrease (P_{atm} peak points in **Fig. 6a**) always precedes the *outflow* events and vice versa. A consistent temporal lag was observed between the P_{atm} peak and the onset of *outflow* events. On average, the decrease in P_{atm} preceded the initiation of *outflow* by ~130 minutes (see **Fig. S4** in the supplementary information), reflecting the delayed response of the subsurface air column to pressure gradients.

In addition, the inverse behavior observed in O_2 concentrations (**Fig. 2b**) supports the presence of advective air transport. During *outflow* events, as CO_2 concentrations increase due to the upward movement of CO_2-rich air from the subsurface, O_2 concentrations concurrently decrease, consistent with a displacement of atmospheric air by subsurface air. This coupled, opposing trend between CO_2 and O_2 is characteristic of bulk, advective air movement.

FFT analysis further confirms that changes in P_{atm} control air dynamics in the dry well (**Fig. 6b**). The power spectrum of the P_{atm} signal reveals a prominent peak at 2 cycles per day, which matches the dominant frequency observed in the CO_2 and O_2 concentration data from both the top and bottom nodes. This spectral coherence strongly suggests that P_{atm} is the primary driver of the air transport in the dry well. In contrast, air temperature shows a peak at one cycle per day, which does not align with the fluctuations in CO_2 and O_2 concentrations. This distinction supports the conclusion that pressure, rather than temperature, is the dominant forcing mechanism for air transport in the case of the dry well.

https://doi.org/10.5194/egusphere-2026-1910
Preprint. Discussion started: 4 May 2026

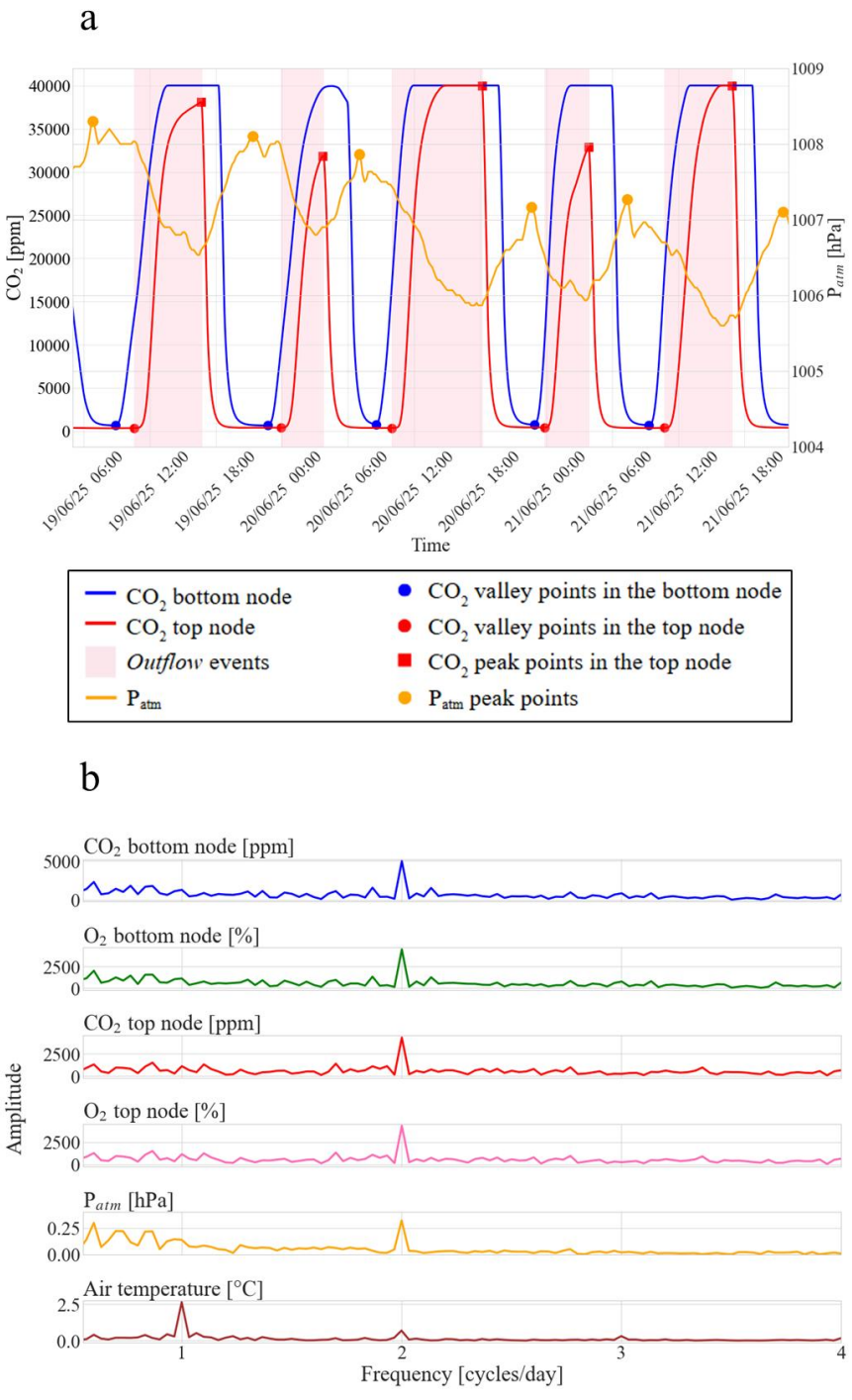

https://doi.org/10.5194/egusphere-2026-1910
Preprint. Discussion started: 4 May 2026

Figure 6: (a) Time series data from three days during summer showcasing the effect of P_{atm} on air dynamics in the dry well. A drop in P_{atm} precedes *outflow* events. (b) FFT analysis of the measured CO_2 and O_2 concentrations from top and bottom nodes, $P_{atm,}$ and air temperature.

Further studies indicate the effect of BP on air transport between the subsurface and the atmosphere. For example, in an experiment conducted in British Columbia, Canada, a subsurface wellbore leakage was simulated (Forde et al., 2017). They found that intervals of decreasing P_{atm} were strongly correlated with increased CH_4 flux into the atmosphere, and, conversely, intervals of increasing P_{atm} were strongly correlated with decreased, and even ceased, CH_4 emissions.

3.4.2. Air stratification and recharge events within the wet well

The air transport mechanisms observed in the wet well differ substantially from those in the dry well, although both are located at the same lithology under the same atmospheric conditions. During the warmer months (April to October), the wet well exhibits clear vertical linear stratification, with elevated CO_2 concentrations at the bottom and near-atmospheric CO_2 levels at the top (**Fig. 3c** and **7c**). This pattern is consistent with thermal stability within the well, as indicated by sustained negative ΔT_V values during the same period (**Fig. 7d**), which suppressed TIC mixing and allowed CO_2 to accumulate in the lower well section.

In contrast, winter months are characterized by a breakdown of this stratification due to multiple contributing factors. The first is the onset of thermal instability, which promotes vertical mixing of air masses within the well column (Perrier and Richon, 2010; Levintal et al., 2018a). The second is specific to infiltration wells and relates to the operational introduction of rainwater. During this infiltration period, increased water input into the well was associated with a rise in the local groundwater table of ~0.1-1 m (**Fig. 7a**). This hydrological change coincided with a decrease in CO_2 concentrations and an increase in O_2 concentrations at the bottom of the well (to below 1000 ppm and above 20 %, respectively). Previous studies indicate that rainwater infiltration can flush or dilute subsurface CO_2 pools (Delsarte et al., 2021) and that rainwater generally contains significantly lower $CO_{2(aq)}$ than groundwater. Therefore, a possible explanation is that the addition of rainwater with low $CO_{2(aq)}$, in contrast to the higher $CO_{2(aq)}$ typically found in groundwater (e.g., **Fig. 7e**, summer months), diluted the $CO_{2(aq)}$ in the groundwater, which is one of the sources for CO_2 in the well shaft above. In the context of infiltration wells, introduction of rainwater may therefore reduce well CO_2 concentrations by dilution, consistent with our observations. It is important to note that although the two wells are located ~7 m apart and have the same soil and atmospheric conditions, no BP was observed in the wet well, unlike in the dry well. This is due to the groundwater table being above the well's perforation depth (i.e., wet well definition), which is considered an impermeable boundary to BP-driven air transport (You et al., 2010).

https://doi.org/10.5194/egusphere-2026-1910
Preprint. Discussion started: 4 May 2026

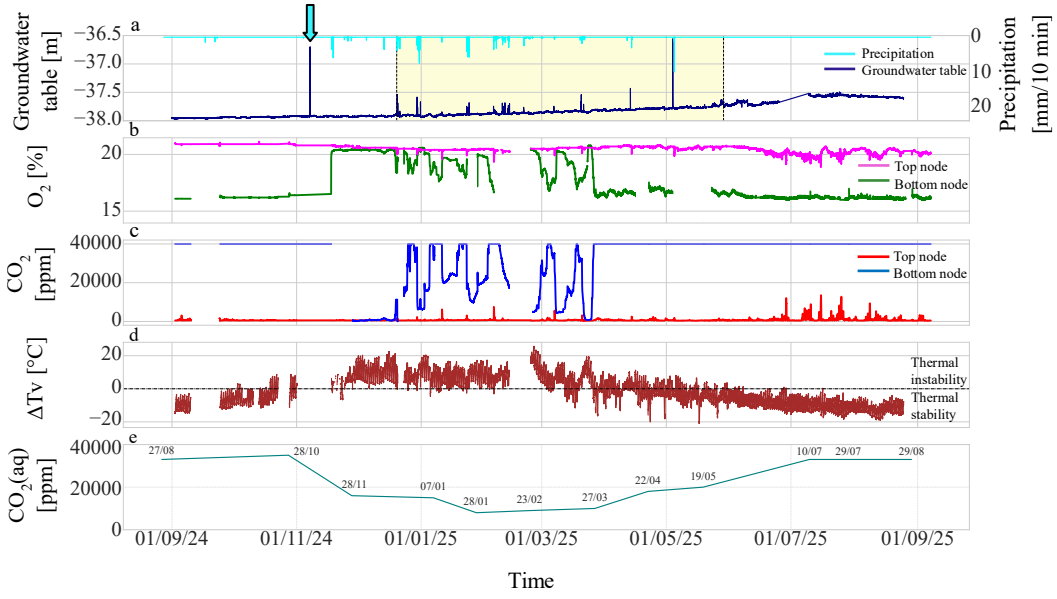

Figure 7: One-year time series data (September 2024 - August 2025) in the wet well. (a) Groundwater table within the well and precipitation. The light blue arrow represents the experimental infiltration conducted on 07/11/2024 and the light yellow background represents the operational infiltration period during winter; (b) O_2 concentrations in the top and bottom nodes; (c) CO_2 concentrations in the top and bottom nodes; (d) ΔT_V between the bottom node and the atmosphere ($T_{V(bottom)} - T_{V(atm)}$) – positive values indicates thermal instability conditions; (e) $CO_{2(aq)}$ in the groundwater measured during the monthly field days (dates of the field days above the bars). Blank areas indicate missing data due to system malfunctions (see section 2.2 for additional details).

3.5. Conceptual model – Air transport mechanisms in dry and wet infiltration wells

To synthesize the above findings, we developed a conceptual model illustrating the dominant mechanisms governing air transport in a dry well vs. a wet well type (**Fig. 8**). The model was developed based on the continuous data obtained from the monitoring systems installed in both wells, complemented by observations collected during field days and supported by previous studies (Li et al., 2022; Levintal et al., 2020b). The model integrates both diurnal and seasonal dynamics, highlighting the contrasting behaviors of the two well types and the key physical processes that control air transport between the subsurface and the atmosphere.

Fig. 8a illustrates the BP mechanism, which was observed only in the dry well. This process is driven by fluctuations in P_{atm}, which induce alternating *inflow* and *outflow* events, as discussed in section 3.4.1. When $dP_{atm}/dt < 0$, air with high CO_2 is drawn from the pore space in the unsaturated zone into the open well section and to the atmosphere (**Fig. 8a,** red arrows), while $dP_{atm}/dt > 0$ initiates air with atmospheric CO_2 concentrations to flow in the opposite direction, from the atmosphere into the well (**Fig. 8a,** blue arrows). The BP mechanism exhibits a diurnal cycle, with an average of two cycles per day (**Fig. 6**);

https://doi.org/10.5194/egusphere-2026-1910
Preprint. Discussion started: 4 May 2026

however, no trends were observed in the dry well on a seasonal scale, as shown in the 1-year time series (**Fig. S4**). The BP mechanism in wells has already been reported in several studies (e.g., Jiang et al., 2023; Li et al., 2022; Neeper, 2003), yet this is the first time it has been compared between two well types (dry vs. wet well) under similar soil and atmospheric conditions.

Fig. 8b and **8c** present the wet well type in which, in contrast to the dry well, seasonal mechanisms govern air transport dynamics without observed diurnal patterns. During the summer season (**Fig. 8b**), thermal stability within the wet well suppresses TIC air mixing, resulting in diffusion as the dominant air transport mechanism. This diffusion-dominated regime promotes vertical stratification of the well air column, as supported by the vertical linear CO_2 decrease in the air column from the groundwater table to the wellhead above (red lines in **Fig. 4b**). During the winter season, air transport in the wet well is influenced by two environmental factors. First, atmospheric cooling induces thermal instability within the well, facilitating TIC and promoting vertical mixing of the well's internal air column. This process leads to a decrease in CO_2 concentrations at the bottom of the well down to atmospheric concentrations of ~420 ppm during large T_V (e.g., **Fig. 7c** and **7d**; see CO_2 values of ~420 ppm at the bottom node during ΔT_V ~20 °C).

Second, rainwater infiltration into the well during operational recharge periods further decreases CO_2 concentrations at depth. Rainwater, typically undersaturated with respect to $CO_{2(aq)}$ compared to groundwater, dilutes $CO_{2(aq)}$ in the groundwater, thereby reducing CO_2 degassing and lowering CO_2 concentration in the well. It is important to emphasize that the seasonal transition between the dominant air transport mechanisms is not abrupt; an intermediate state occurs, mainly during spring. It's a transient stage in which the TIC is developed from above, causing two distinct sub-sections with a transient layer at ~-15 m: an upper TIC-driving mixing layer and a lower diffusion-driving vertical gradient (green lines in **Fig. 4b**).

This conceptual model indicates the seasonal stratification and TIC observed in the wet well compared to the diurnal BP mechanism active in the dry well, emphasizing the roles of both well type and atmospheric forcing in controlling air transport. It highlights the importance of considering both temporal scales (diurnal vs. seasonal) and structural types (wet vs. dry) when evaluating the potential for gas exchange between subsurface environments and the atmosphere via wells.

From an environmental perspective, the dry well exhibits higher CO_2 emissions than the wet well, primarily due to the dominance of advective transport driven by BP, compared to the more diffusion-dominated transport (with a minor seasonal TIC addition) in the wet well. Although the CO_2 fluxes measured in this study were relatively low (**Fig. 5**) and thus associated with minimal environmental impact, these findings may not be representative of all well systems. In shallow wells that are directly open to the atmosphere and strongly influenced by P_{atm} fluctuations, CO_2 emissions may be substantially higher and could contribute meaningfully to atmospheric GHG concentrations. Moreover, site-specific factors such as soil type, higher GHG concentrations in groundwater or the unsaturated zone, climatic conditions, and wellhead geometry (e.g., diameter) are likely to modulate the magnitude of gas emissions, potentially leading to greater environmental impacts in other settings.

https://doi.org/10.5194/egusphere-2026-1910
Preprint. Discussion started: 4 May 2026

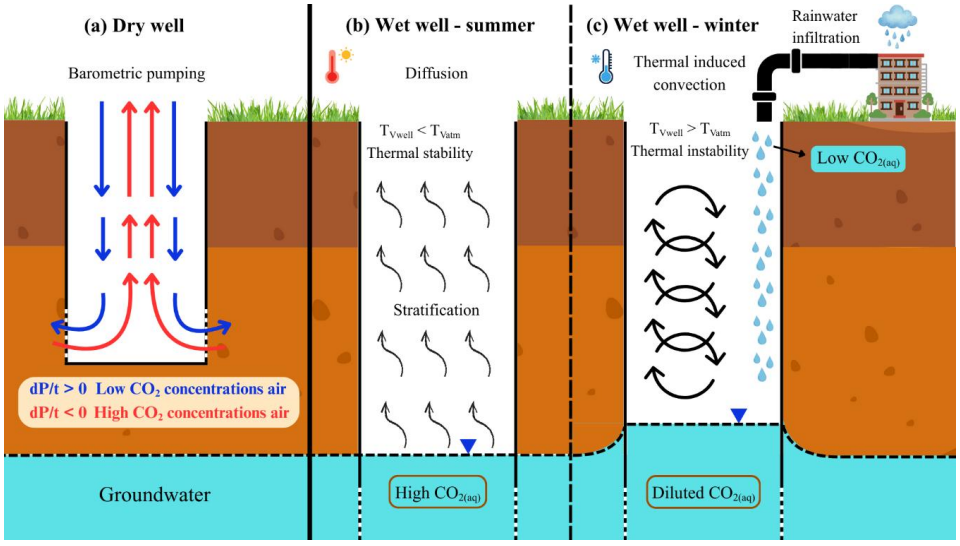

Figure 8: Conceptual model of the mechanisms controlling air transport within (a) a dry well, (b) a wet well in summer, and (c) a wet well in winter**.** The dashed horizontal line and blue triangle indicate the groundwater table. The dashed vertical lines at the bottom of both wells represent the perforated sections. Low CO_2 concentrations are ~420 ppm, and high CO_2 concentrations are site-dependent (in our case, ~40000 ppm).

4. Conclusions

This study presents a novel comparison of air transport mechanisms in two types of infiltration wells under identical climatic and soil conditions, using high-resolution monitoring of CO_2 and O_2. One well at a depth of 47 m, which reaches below the groundwater table (a wet well), and a second well at a depth of 27 m, which reaches the unsaturated zone, above the groundwater table (a dry well). In both wells, sensors were installed at the top of the well (-1 m) and at the bottom of the wet well (-30 m) and the dry well (-20 m), measuring CO_2 and O_2 concentrations, temperature, and relative humidity every minute for one year. The main objectives of the study were to compare the air transport mechanisms of the two wells and to examine the potential for CO_2 emissions from the wells to the atmosphere.

The dry well exhibits clear, dynamic semi-diurnal fluctuations in gas concentrations, strongly coupled with barometric pressure changes, indicating active barometric pumping. In contrast, the wet well displays a more stratified gas profile with limited temporal variability, driven by thermal gradients and recharge operations. The dry well data suggest that barometric pressure fluctuations facilitate alternating *inflow* and *outflow* events, effectively ventilating the subsurface through the well's perforated section. This mechanism results in high-amplitude cycles of CO_2 accumulation and O_2 depletion, followed by rapid atmospheric renewal. In the wet well, however, persistent water saturation suppresses barometric-driven exchange and promotes vertical stratification of gases, especially during warmer months. Winter-

https://doi.org/10.5194/egusphere-2026-1910
Preprint. Discussion started: 4 May 2026

time thermal instability and recharge events, on the other hand, disrupt stratification and promote mixing, thereby lowering CO_2 concentrations.

The CO_2 flux from the dry well was greater than that from the wet well, due to the mechanisms controlling each well. The CO_2 flux from the dry well to the atmosphere was minor, despite the high concentrations measured during the *outflow* events, due to low air velocities within the well. However, when scaled up to hundreds or thousands of wells, even a flux of this magnitude could be significant.

Data availability

The dataset used in the analyses can be found in the Supplement to this article.

Author contributions

EL, AG, and EL conceptualized and conducted the study and wrote the first draft of the manuscript. AG and EL provided the resources. UN and LN helped with developing the methodology and data. EL, AG, UN, and EL contributed to the final version.

Competing interests

The authors declare that they have no conflict of interest.

Acknowledgements

The authors thank Elyasaf Freiman, Ariel Altman, Thi Thuc Nguyen, Devi Orozco, and Roee Katzir for their help with the fieldwork, and Neta Soto for her help with the conceptual model.

Financial support

EL was supported by the Interdisciplinary Scholarship for Master's students in Research Track at Ben-Gurion University of the Negev.

https://doi.org/10.5194/egusphere-2026-1910
Preprint. Discussion started: 4 May 2026

5. References

Bourges, F., Genthon, P., Genty, D., Lorblanchet, M., Mauduit, E., & d'Hulst, D. (2014). Conservation of prehistoric caves and stability of their inner climate: Lessons from Chauvet and other French caves. *Science of the Total Environment*, *493*, 79-91.

Delsarte, I., Cohen, G. J., Momtbrun, M., Höhener, P., & Atteia, O. (2021). Soil carbon dioxide fluxes to atmosphere: The role of rainfall to control CO_2 transport. *Applied Geochemistry*, *127*, 104854.

Dhanu Radha, S. V. V., Sabarathinam, C., Al-Ayyadhi, N., Al-Ajeel, F. K., Al-Qallaf, H., & Akber, A. (2022). Spatial and temporal variation of dissolved CO_2 in rainwater from an arid region with special focus on its association with DIC and pCO_2. *Environmental Earth Sciences*, *81*(4), 113.

Du, Y., Guo, S., Wang, R., Song, X., & Ju, X. (2023). Soil pore structure mediates the effects of soil oxygen on the dynamics of greenhouse gases during wetting–drying phases. *Science of The Total Environment*, *895*, 165192.

Dumitru, O. A., Onac, B. P., Fornós, J. J., Cosma, C., Ginés, A., Ginés, J., & Merino, A. (2015). Radon survey in caves from Mallorca Island, Spain. *Science of the Total Environment*, *526*, 196-203.

Forde, O. N., Cahill, A. G., Beckie, R. D., & Mayer, K. U. (2019). Barometric-pumping controls fugitive gas emissions from a vadose zone natural gas release. *Scientific Reports*, *9*(1), 14080.

Ganot, Y., Dragila, M. I., & Weisbrod, N. (2012). Impact of thermal convection on air circulation in a mammalian burrow under arid conditions. *Journal of Arid Environments*, *84*, 51-62.

Ganot, Y., Dragila, M. I., & Weisbrod, N. (2014). Impact of thermal convection on CO_2 flux across the earth–atmosphere boundary in high-permeability soils. *Agricultural and Forest Meteorology*, *184*, 12-24.

Góra, A., Sechman, H., Guzy, P., & Twaróg, A. (2018). Measurements of methane and carbon dioxide emissions around the boreholes. *International Multidisciplinary Scientific GeoConference: SGEM*, *18*(5.2), 633-640.

Jiang, J., Gu, K., Xu, J., Li, Y., Le, Y., & Hu, J. (2023). Effect of barometric pressure fluctuations on gas transport over soil surfaces. *Land*, *12*(1), 161.

Kang, M., Christian, S., Celia, M. A., Mauzerall, D. L., Bill, M., Miller, A. R., ... & Jackson, R. B. (2016). Identification and characterization of high methane-emitting abandoned oil and gas wells. *Proceedings of the National Academy of Sciences*, *113*(48), 13636-13641.

Kang, M., Kanno, C. M., Reid, M. C., Zhang, X., Mauzerall, D. L., Celia, M. A., ... & Onstott, T. C. (2014). Direct measurements of methane emissions from abandoned oil and gas wells in Pennsylvania. *Proceedings of the National Academy of Sciences*, *111*(51), 18173-18177.

https://doi.org/10.5194/egusphere-2026-1910
Preprint. Discussion started: 4 May 2026

Lebel, E. D., Lu, H. S., Vielstädte, L., Kang, M., Banner, P., Fischer, M. L., & Jackson, R. B. (2020). Methane emissions from abandoned oil and gas wells in California. *Environmental Science & Technology*, *54*(22), 14617-14626.

Levintal, E., Dragila, M. I., Lensky, N. G., & Weisbrod, N. (2018). Mechanisms controlling air stratification within a large diameter borehole and atmospheric exchange. *Journal of Geophysical Research: Earth Surface*, *123*(12), 3251-3268.

Levintal, E., Dragila, M. I., Lensky, N. G., & Weisbrod, N. (2020). Borehole diameter controls thermal-induced convection and evaporation from a shallow water table. *Geophysical Research Letters*, *47*(18), e2020GL089411.

Levintal, E., Dragila, M. I., Zafrir, H., & Weisbrod, N. (2020). The role of atmospheric conditions in CO_2 and radon emissions from an abandoned water well. *Science of the Total environment*, *722*, 137857.

Levintal, E., Lensky, N. G., Mushkin, A., & Weisbrod, N. (2018). Pipes to Earth's subsurface: The role of atmospheric conditions in controlling air transport through boreholes and shafts. *Earth System Dynamics*, *9*(3), 1141-1153.

Li, H., Liu, W., Zhan, H., Sun, S., Wang, X., Wang, S., ... & Wang, X. (2022). Effect of barometric pumping on relative humidity in the loessal soil of the loess Plateau. *Geoderma*, *424*, 116008.

Liang, X., Zhan, H., & Zhang, Y. K. (2018). Aquifer recharge using a vadose zone infiltration well. *Water Resources Research*, *54*(11), 8847-8863.

Liñán, C., Vadillo, I., Benavente, J., Cañete, S., & Ojeda, L. (2025). Fluctuations of CO_2 and 222Rn concentration in the karst vadose zone: Comparing exhalation, indoor concentrations, and cave air dynamics (Nerja Cave, Southern Spain). *Science of the Total Environment*, *984*, 179723.

Lionello, P., Malanotte-Rizzoli, P., Boscolo, R., Alpert, P., Artale, V., Li, L., ... & Xoplaki, E. (2006). The Mediterranean climate: an overview of the main characteristics and issues. *Developments in earth and environmental sciences*, *4*, 1-26.

Macpherson, G. L. (2009). CO_2 distribution in groundwater and the impact of groundwater extraction on the global C cycle. *Chemical Geology*, *264*(1-4), 328-336.

Massmann, J., Shock, S., & Johannesen, L. (2000). Uncertainties in cleanup times for soil vapor extraction. *Water Resources Research*, *36*(3), 679-692.

Minamikawa, K., Nishimura, S., Sawamoto, T., Nakajima, Y., & Yagi, K. (2010). Annual emissions of dissolved CO_2, CH_4, and N_2O in the subsurface drainage from three cropping systems. *Global change biology*, *16*(2), 796-809.

Misstear, B., Banks, D., & Clark, L. (2017). *Water wells and boreholes*. John Wiley & Sons.

https://doi.org/10.5194/egusphere-2026-1910
Preprint. Discussion started: 4 May 2026

Monteiro, E., & Torlaschi, E. (2007). On the dynamic interpretation of the virtual temperature. *Journal of the atmospheric sciences*, *64*(8), 2975-2979.

Morais, T. A., & Ryan, M. C. (2023). In-Well Degassing of Monitoring Wells Completed in Gas-Charged Aquifers. *Groundwater*, *61*(1), 86-99.

Mourzenko, V. V., Varloteaux, C., Guillon, S., Thovert, J. F., Pili, E., & Adler, P. M. (2014). Barometric pumping of a fractured porous medium. *Geophysical Research Letters*, *41*(19), 6698-6704.

Nachshon, U., Weisbrod, N., & Dragila, M. I. (2008). Quantifying air convection through surface-exposed fractures: A laboratory study. *Vadose Zone Journal*, *7*(3), 948-956.

National Ground Water Association. (n.d.). *Groundwater Facts*. NGWA. https://www.ngwa.org/what-is-groundwater/About-groundwater/groundwater-facts.

Neeper, D. A. (2003). Harmonic analysis of flow in open boreholes due to barometric pressure cycles. *Journal of contaminant hydrology*, *60*(3-4), 135-162.

Netzer, L., Kurtzman, D., Ben-Hur, M., Livshitz, Y., Katzir, R., & Nachshon, U. (2024). Novel approach to roof rainwater harvesting and aquifer recharge in an urban environment: Dry and wet infiltration wells comparison. *Water Research*, *252*, 121183.

Netzer, L., Russo, D., Nachshon, U., Moreno, Z., Ben-Hur, M., Katzir, R., ... & Kurtzman, D. (2025). Drywell infiltration performance: Tests, monitoring, simple, and detailed models. *Water Resources Research*, *61*(2), e2024WR037524.

Perrier, F., & Le Mouël, J. L. (2016). Stationary and transient thermal states of barometric pumping in the access pit of an underground quarry. *Science of the Total Environment*, *550*, 1044-1056.

Perrier, F., & Richon, P. (2010). Spatiotemporal variation of radon and carbon dioxide concentrations in an underground quarry: coupled processes of natural ventilation, barometric pumping and internal mixing. *Journal of Environmental Radioactivity*, *101*(4), 279-296.

Rossabi, J., & Falta, R. W. (2002). Analytical solution for subsurface gas flow to a well induced by surface pressure fluctuations. *Groundwater*, *40*(1), 67-75.

Ryan, M. C., MacQuarrie, K. T. B., Harman, J., & McLellan, J. (2000). Field and modeling evidence for a "stagnant flow" zone in the upper meter of sandy phreatic aquifers. *Journal of Hydrology*, *233*(1-4), 223-240.

Sánchez-Cañete, E. P., Serrano-Ortiz, P., Domingo, F., & Kowalski, A. S. (2013). Cave ventilation is influenced by variations in the CO_2-dependent virtual temperature. *International Journal of Speleology*, *42*(1), 1.

Seibt, U., Brand, W. A., Heimann, M., Lloyd, J., Severinghaus, J. P., & Wingate, L. (2004). Observations of O_2: CO_2 exchange ratios during ecosystem gas exchange. *Global Biogeochemical Cycles*, *18*(4).

https://doi.org/10.5194/egusphere-2026-1910
Preprint. Discussion started: 4 May 2026

Slade, G. W. (2013). The fast fourier transform in hardware: A tutorial based on an FPGA implementation. *Mar*, *21*, 1-26.

Smagin, A. V., & Karelin, D. V. (2021). Effect of wind on soil-atmosphere gas exchange. *Eurasian soil science*, *54*(3), 372-380.

Smith, K. A., Ball, T., Conen, F., Dobbie, K. E., Massheder, J., & Rey, A. (2018). Exchange of greenhouse gases between soil and atmosphere: interactions of soil physical factors and biological processes. *European journal of soil science*, *69*(1), 10-20.

Weisbrod, N., Dragila, M. I., Nachshon, U., & Pillersdorf, M. (2009). Falling through the cracks: The role of fractures in Earth-atmosphere gas exchange. *Geophysical Research Letters*, *36*(2).

Xiong, Y., Zhou, Z., Huang, Y., Ding, S., Wang, X., Wang, J., ... & Wei, H. (2025). CO_2 Dynamics and Transport Mechanisms Across Atmosphere–Soil–Cave Interfaces in Karst Critical Zones. *Geosciences*, *15*(10), 376.

You, K., Zhan, H., & Li, J. (2010). A new solution and data analysis for gas flow to a barometric pumping well. *Advances in water resources*, *33*(12), 1444-1455.

You, K., Zhan, H., & Li, J. (2011). Gas flow to a barometric pumping well in a multilayer unsaturated zone. *Water Resources Research*, *47*(5).